Isobavachalcone Attenuates NLRP3 Inflammasome-related Pyroptosis and Induces Apoptosis via Arresting Cell Cycle in Glioblastoma

Yueshan Wu
Hubei University Of Science and Technology
Jing Chang
Hubei University Of Science and Technology
Juanjuan Ge
Hubei University Of Science and Technology
Kangyan Xu
Hubei University Of Science and Technology
Quan Zhou
Hubei University Of Science and Technology
Xiaowen Zhang
Hubei University Of Science and Technology
Ni Zhu (zhuni@whu.edu.cn)
Hubei University Of Science and Technology https://orcid.org/0000-0003-3294-5167
Meichun Hu
Hubei University Of Science and Technology

Research Article

Keywords: Glioblastoma, Isobavachalcone, NLRP3, Pyroptosis, Apoptosis, Cell cycle

Posted Date: March 16th, 2022

DOI: https://doi.org/10.21203/rs.3.rs-1416834/v1

Abstract

Glioblastoma (GBM) is the worst and most common malignant intracranial tumor with high mortality rates and almost invariably poor prognosis even after surgery, radiotherapy, chemotherapy and emerging immunotherapies. Therefore, it is important to find new therapeutic drugs for GBM treatment. In the present study, we aimed to explore the effect of one natural chalcone—Isobavachalcone (IBC) on GBM and clarify its anti-cancer mechanisms. It was observed that IBC could inhibit GBM cell proliferation, migration and invasion *in vitro* and prevent tumor growth without any significant drug toxicity *in vivo*. Mechanistically, IBC may target NOD-like receptor family pyrin domain-containing 3 (NLRP3) transcription factor estrogen receptor 1 (ESR1) by network pharmacology and molecular docking analysis. Experimentally, IBC reduced NLRP3 inflammasome-related pyroptosis and inflammation, arrested cell cycle at G1 phase, and induced mitochondria-dependent apoptosis in GBM cells. These results indicated that IBC is a potential therapeutic drug against GBM and provide a new insight into GBM treatment.

Introduction

Glioblastoma (GBM) is the most common and lethal malignant brain tumor with high molecular heterogeneity, poor overall prognosis and a meagre 10-year survival rate less than 1% [1, 2]. Current treatment strategy of GBM involves surgical resection in combination with adjuvant chemoradiotherapy, and most recently the addition of immunotherapies in gliomas[3, 4]. However, because of the inherent infiltrative nature of GBM and unclear demarcation between tumors and normal brain tissues, surgical resection rarely results in removal of all tumor tissue completely[5]. Subsequently, the recurrence after surgery and higher glioma malignance occur frequently due to the rapidly proliferation of GBM cells and high diffusion throughout the brain[6]. Moreover, GBM has easy resistance to radiotherapy and classic chemotherapy drugs due to be hindered by blood-brain barrier (BBB), so the therapeutic efficacy of GBM drugs are usually limited[7]. For instance, the resistance of temozolomide (TMZ), which is a standard chemotherapeutic option for the treatment of GBM, seems inevitable, resulting in GBM treatment failure[8]. Therefore, it is vital to develop new anti-GBM drugs that could readily cross the BBB, effectively inhibit cancer cell growth, as well as exhibit relatively lower toxicity.

Isobavachalcone (IBC), a natural prenylated chalcone, is one of the main ingredients of *Psoralea corylifolia Linn* seeds, demonstrating anti-cancer, anti-microbial, anti-inflammatory, neuroprotective and other remarkable pharmacological activities[9]. It had been reported that IBC inhibited several cancers growth, such as leukemia, colorectal cancer, liver cancer, breast cancer, prostate cancer, gastric cancer, cervical cancer, neuroblastoma and so on[9]. However, the inhibitory effect of IBC on GBM has not been clarified adequately. Several early studies revealed IBC could be quickly absorbed into rat plasma and distribute almost evenly to the cerebral nuclei, suggesting IBC could cross the BBB and preserve in brain [10]. These characteristics of IBC made it to be a potential drug to treat diverse central nervous system (CNS) diseases, such as Alzheimer's and Parkinson's disease and the GBM, one of the most frequent primary malignant CNS tumor [11, 12].

In the present study, IBC was found to inhibit GBM cell proliferation, migration and invasion *in vitro* and suppress tumor growth with no obvious adverse effects *in vivo*. The network pharmacology and molecular docking analysis revealed that IBC may target NLRP3 transcription factor ESR1. Further experiments confirmed that IBC reduced NLRP3 inflammasome-related pyroptosis in GBM cells. Meanwhile, IBC arrested cell cycle at G1 phase via p53/p21/CDK2 pathway and induced mitochondria-dependent apoptosis of GBM. These results demonstrated that IBC might be promising therapeutic candidates for GBM treatment.

Materials And Methods

Reagents and Cell Culture

The drugs, IBC (CAS: 20784-50-3) and temozolomide (TMZ, CAS: 20784-50-3), was purchased from Shanghai Yuanye Bio-Technology Co., Ltd, and Shanghai Aladdin Biochemical Technology Co., Ltd, respectively. Pan-caspase inhibitor Z-VAD-FMK (CAS: 161401-82-7) was purchased from MedChemExpress LCC.

Human GBM cell lines, U87MG and U251 were purchased from the American Type Culture Collection. These two cell lines were cultured in Dulbecco's modified Eagle's medium (DMEM, Gibco, CA, USA) supplemented with 10% fetal bovine serum (FBS, Gibco, America) and 1% penicillin/streptomycin. All cells were incubated in a 5% CO_2 incubator at 37°C for indicated time.

Cell Viability Analysis

The MTT assay was used to measure cell proliferation according to manufacturer's instructions[13]. Cells were cultured in 96-well plates (3×10^3 cells/well) at 37°C with indicated compounds for 48 h, followed by 10 μL of MTT reagent and incubated for 1h. OD value was measured according to the wavelength of 570 nm using a Multi-Mode Reader (BioTek Instruments, Inc.,USA.). The biochemical half maximal inhibitory concentration (IC_{50}) values were calculated using GraphPad Prism 8 software (GraphPad Software Inc., San Diego, CA, USA).

A total of 3×10^3 cells/well were seeded in 96-well plates and allowed to attach overnight. U87MGand U251 cells were pretreated with 45 μL Z-VAD-FMK for 30 min to block caspase activity. Then U87MG and U251 cells were treated with different concentration of IBC for 48 h, followed by 10 μL of CCK-8 reagent and incubated for 1 h. OD value was measured wavelength of 450 nm using a Multi-Mode Reader. Then we followed the above method to measure cell proliferation.

Colony Formation Assay

GBM cells were seeded 1000 cells per well in 6-well plates (Costar, Corning, NY, USA), and cultured with indicated concentrations of IBC at 37°C for 7 days. Then the plates were fixed with methanol and stained with 1% crystal violet for at least 30 min. After staining, extra dye was washed, and the colonies were imaged and counted[14].

Wound Healing Assay

Wound healing (scratch) assays was performed according to standard protocol[15]. Briefly, U87MG and U251 cells were seeded in 6-well plates (1.5×10^6 cells per well). The second day, cells were scratched by a sterile 200 μL pipette tip followed by washing with PBS twice to remove cellular debris, and then cultured under indicated doses of IBC. The cell were visualized by light microscopy and the width of the wound was measured after IBC treatment at 0 h and 48 h. The cell migration rates were calculated by the ratio of the migration distance in IBC treating groups to the control group.

Cell Migration and Invasion Assays

Transwell (#3422, Corning Costar, Carlsbad, CA, USA) was used to detect the effects of IBC on migration and invasion of U87MG and U251 cells. 5×10^4 cells in 200 μL of serum-free medium were placed in the upper chamber of 24-well transwell insert. Subsequently, 600 μL of DMEM supplemented with 10% FBS was added to the lower chamber. Assaying cell invasion, the cells were seeded into the upper chamber after the bottom of the transwell insert was covered with Matrigel (1:8 dilution, Corning Biocoat, USA)[16]. The following steps were identical to the migration assay. After incubation for 48 h, Cells that passed through the transwell membrane were fixed with 4% paraformaldehyde for 20 min before being stained with 1% crystal violet for 20 min. Then the cells in five random views were counted under the X71 fluorescence microscope (magnification, ×200, Olympus Corporation).

Cell Cycle Assay

Cells were plated and treated using different concentrations of IBC for 48 h. Then cells were harvested and fixed in 70% ethanol overnight at 4°C. The fixed cells were rinsed in PBS and then hydrolyzed with RNase (100 g/ml) and 0.2% Triton X-100 for 30 min at 37°C. After treatment, the cells were rinsed in PBS and stained in the dark with Propidium Iodide (PI) (50 μg/mL) for 30 min[17]. The cell cycle distribution was measured by a flow cytometer (CytoFLEX S, Beckman Coulter, Fullerton, CA, USA).

Hoechst 33342 Staining

GBM cells in the logarithmic growth phase were subjected to Hoechst 33342 staining. Briefly, 3×10^4 GBM cells were seeded into 96-well plates and incubated overnight at 37°C. After IBC treatment for 48 h, the cells were rinsed in PBS and stained with 100 μL Hoechst 33342 (10 μg/ml) in the dark for 30 min[18]. After PBS rinsing, the cells were observed under fluorescence microscope.

Annexin V-FITC/PI Double Staining Assay

The Annexin V-FITC/Propidium Iodide (PI) double staining assay was used to evaluate the apoptosis in U87MG and U251. Results can be observed by fluorescence microscope or flow cytometer. GBM Cells were treated with different concentration of IBC for 48 h. Cells were resuspended in trypsin and washed twice with ice-cold PBS. Then, Annexin V-FITC/PI double staining was performed according to the instructions of the Annexin V-FITC/PI apoptosis detection kit (C1067M, Beyotime, Shanghai, China). Each

sample was scanned by a flow cytometer and analyzed by FlowJo 7.6. Alternatively, samples were observated by fluorescence microscopy. The procedure for processing cells is the same as with flow cytometry.

Mitochondrial Transmembrane Potential (ΔΨm) Assay

Mitochondrial tansmembrane potential (MTP, ΔΨm) assay kit (Biosharp, Shanghai, China) was used to assess MTP (ΔΨm) in GBM cells after IBC treatment. U87MG and U251 cells were seeded in 6-well plates for 24 h and then treated with indicated doses of IBS for 48 h. Then GBM cells were stained with the JC-1 probe in the dark for 30 min. After PBS rinsing, the cells were observed under fluorescence microscope and the J- aggregates were detected using an excitation wavelength of 585 ~ 590 nm, and monomer of 515 ~ 529 nm, respectively.

Western Blot Analysis

The IBC-treated cells were lysed in RIPA buffer (P003B, Beyotime, Shanghai, China) for 30min incubation on ice. After mixing and centrifugation at 13000 g for 20min at 4°C, the protein supernatants were collected and proteins were quantified by BCA protein quantification kit (P0012S, Beyotime, Shanghai, China). Then the proteins were separated by 10% SDS-polyacrylamide gel electrophoresis (P0012A, Beyotime, Shanghai, China) and transferred to a nitrocellulose membrane (Millipore, USA). Subsequently, the membrane was blocked with 5% BSA for 1 h and successively with indicated primary antibody overnight at 4°C and then an HRP-conjugated secondary antibody (1:1000, ABclonal, Wuhan, China) at 37°C for 1 h. The Ultrasensitive ECL chemiluminescence kit (P0018AS, Beyotime, Shanghai, China) was used to detect proteins, and Image J for Windows from the National Institutes of Health (NIH) (Bethesda, MD, USA) was used to statistically analyze. GAPDH was used as a control. The antibodies used for western blot were as follows: rabbit polyclonal antibodies against NF-κB p65 (1:1000, ABclonal, A19653), NLRP3 (1:1000, ABclonal, A12694), IL-18 (1:1000, Beyotime, AF5207), ASC / TMS1 (1:1000, ABclonal, A1170), p21 (1:1000, ABclonal, A1483), and CDK2 (1:1000, ABclonal, A0294), Phospho-EGFR-Y1068 (1:1000, ABclonal, AP0301), Phospho-GSK3β (1:1000, ABclonal, AP0039), GSK3β(1:1000, ABclonal, A3174), Phospho-Akt (1:1000, ABclonal, AP1259), AKT (1:1000, ABclonal, A11016), Bax (1:1000, ABclonal, A12009), TNF-α (1:1000, ABclonal, A11534), IL1β(1:1000, ABclonal, A11370), Bcl-2 (1:1000, ABclonal, A0208), Cleaved-Caspase 3 (1:1000, ABclonal, A19654), Caspase 1 (1:1000, ABclonal, A0964), GSDMD (1:1000, ABclonal, A20197), a mouse monoclonal antibody against p53 (1:1000, ABclonal, A10610), and HRP Goat Anti-Rabbit IgG(1:1000, ABclonal, AS014), HRP Goat Anti- Mouse IgG (1:1000, ABclonal, AS003).

GBM Subcutaneous Xenograft Model

GBM Xenograft model were established as described previously[19]. Eight-weeks-old BALB/c nude mice were obtained from Beijing Vital River Laboratory Animal Technology Co., Ltd. and then raised in the SPF Laboratory Animal room. After deep anesthesia, 5×10^6 U87MG cells in 100 μL sterile PBS were injected into the subcutaneous. When the tumors had reached an average volume of roughly 100 mm^3, the mice

were randomly distributed into three groups, including control group (n = 10), low group (n = 10) and high group (n = 10). For control group, they only received DMSO daily by intragastric administration (i.g.) for 14 days. The low and high group mice were intragastrically administrated daily with 20 mg/kg or 40 mg/kg IBC for 14 days. During the IBC intragastric administration period, tumor volumes were recorded every 2 days, while body weights were measured daily. Tumor volume was calculated by the following formula: volume = $a \times b^2 \times 0.52$ (whereas a = length and b = width in mm). 14 days later, the mice were sacrificed, and samples of xenograft mice in all groups were collected and prepared for further experiments. In particular, all animal experiments were approved by the Animal Ethics Committee of Hubei University of Science and Technology, and were performed in accordance with institutional and international guidelines for animal care and use.

Hematoxylin and Eosin (HE) and Immunohistochemistry

Dehydrated tissues, fixed in 4% paraformaldehyde, were paraffin embedded and sectioned into 4 μm sections. The tissue blocks were deparaffinized, rehydrated, and stained with hematoxylin and eosin (BL700A, Biosharp, Shanghai, China). The sections were viewed under a microscope after being put on coverslips. To suppress endogenous peroxidase activity, tissue sections were deparaffinized, rehydrated, and treated in 3 percent hydrogen peroxide for immunohistochemical staining. The slides were then antigen-retrieved in citrate buffer (pH 6.0). The tissue pieces were blocked and permeabilized with 0.1% Triton-X 100 after they had been allowed to cool to room temperature. The slices were processed overnight in a humidified chamber at 4°C with CD31 (1:100, Cell Signaling Technology, 3528), Ki67, CD31, Cleaved-Caspase 3 (1:100, Affinity, AF7022), and Ki67 (1:100, Beyotime, AF1738) antibodies. After that, HRP-conjugated secondary antibody was added for 1 h at room temperature. Antibodies were found using the substrate diaminobenzidine (DAB, Beyotime, Shanghai, China), and the slides were counter-stained with hematoxylin (BL700A, Biosharp, Shanghai, China).

Network Pharmacology Analysis

The IBC molecular structure was obtained from Pubchem (https://pubchem.ncbi.nlm.nih.gov/) in the international chemical identifier (InChI) or simplified molecular-input line-entry system format (SMILES). SwissTargetPrediction database (www.swisstargetprediction.ch/) was used to predict relevant targets of IBC for Homo sapiens based on its chemical structure. The GBM disease-related targets were retrieved from the GeneCards (https://www.GeneCards.org/) database by using the keywords “glioma”. Then, the predictive protein targets of IBC against GBM were filtered by Venny 2.1.0 (https://bioinfogp.cnb.csic.es/tools/venny/). According to Gene Ontology (GO) and Kyoto Encyclopedia of Genes and Genomes (KEGG) annotation, the functional and pathway enrichment analyses of overlapped IBC-GBM targets were performed by R (v.3.6.3) software. The protein-protein interaction network (PPI) of the overlapped IBC-GBM targets were constructed by STRING (https://string-db.org/) and Cytoscape v3.8.0 software[20]. The cytoHubba[21], one of plug-in in Cytoscape, was used to predict the protein nodes and sub-network. The IBC-Targets-pathways network was also constructed by Cytoscape v3.8.0 software. The interaction network of NLRP3 transcription factors (TF) was obtained in Gene

Regulatory Networks. The targets of IBC-GBM-NLRP3 TFs were screened out by taking an intersection of IBC-related targets, GBM-related targets and predictive NLRP3 TFs, using Venny 2.1.0.

Molecular Docking

Autodock-VINA[22] and PyMOL software (The PyMOL Molecular Graphics System, Schrödinger, LLC.) were used for molecular docking to analyze the target of IBC target network with moderate value ranking TOP 3, and the target protein database ID was found. The PDB format files of three target proteins were obtained from RSCB PDB database (https://www.rcsb.org/), including ESR1 (PdB-ID: 5E19), Akt1 (PdB-ID: 6HHG) and EGFR (PdB-ID: 6VHN). The SDF format file of IBC was downloaded and selected from PubChem database (https://pubchem.ncbi.nlm.nih.gov/). The target proteins were dehydrated and hydrogenated by Auto Dock software, and the IBC and target proteins were transformed into PDBQT format. Molecular docking was performed by AutoDock program (binding energy less than 0 indicates that the fitness spontaneously binds to the receptor). Finally, PyMOL software was used to visualize the molecular docking results.

Statistical Analysis

The data were statistically analysed using SPSS27.0 software (SPSS, Chicago, IL, USA). Results are presented as mean ± SD. All figures were graphed by GraphPad Prism 8.0 software (GraphPad Software, La Jolla, CA, United States). One-way analysis of variance (ANOVA) with Tukey's post hoc test and two-way RM ANOVA with Sidak's multiple comparisons test were performed to compare differences. Statistical significance was set at $p < 0.05$.

Results

IBC inhibited GBM cells proliferation, migration and invasion

To explore the anti-GBM activity of IBC *in vitro*, two typical human-derived GBM cell lines, U87MG and U251, were used to the cell viability assay. The results showed IBC inhibited U87MG and U251 cells proliferation in a dose-dependent manner (Fig. 1a ~ b). The IC_{50} values of IBC for GBM cells at 48 h were 4.385 μM in U87MG and 1.943 μM in U251 cells, respectively. For TMZ, a positive control for anti-GBM drug, the IC_{50} value were 224.5 μM in U87MG and 472.6 μM in U251 cells, significantly higher than that of IBC (Fig. 1d ~ e). The morphological alterations of GBM cells, such as bubbles, shrank, unclearly visible boundaries, varying cell sizes and loss of cell-cell junctions, were observed in GBM cells with the treatment of IBC (Fig. 1c) and TMZ (Fig. 1f). Moreover, as compared to control group, Colony formation were also significantly reduced in U87MG treated with 1 and 2 μM IBC (Fig. 1g, i) and U251 treated with 0.5 and 1 μM IBC (Fig. 1h, j). In addition, both scratch wound healing assay (Fig. 1k ~ n) and transwells assay (Fig. 1o ~ t) revealed that the migration and invasion of U87MG and U251 cells were significantly inhibited by IBC in a dose-dependent manner. Shortly, IBC could significantly suppressed the proliferation, migration and invasion of GBM cells in a dose-dependent manner.

IBC exerted anti-GBM activity in vivo.

To further confirm the inhibitory effect of IBC on GBM *in vivo*, IBC was performed in nude mice xenograft models. An overview of the experimental workflow was illustrated in Fig. 2a. These results showed low (20 mg/kg) and high (40 mg/kg) dose IBC groups had less tumor sizes, volume and weight than that of the control group since day 8 after treatment initiation (Fig. 2b ~ e). The body weights of both IBC groups became more stability, while body weights in control group declined rapidly with time (Fig. 2f). For tumor vessels, vascular area and angiogenesis in tumor were decreased gradually with increasing IBC dose (Fig. 2g). Drug toxicity is consistently another important factor limiting effective drug development. IBC toxicity in vivo were also assessed in this study. Figure 2h ~ i showed low and high dose IBC-treated mice had no significant differences in both liver morphology and liver/body ratio. In addition, the major organs of IBC-treated mice, such as heart, liver, spleen, lung and kidney, were also stained with HE staining for histological analysis of drug toxicity (Fig. 2j). Histological analysis revealed that IBC treatment did not result in remarkable alterations in these tissues, suggesting IBC was safety for GBM treatment. Moreover, immunohistochemical (IHC) analysis was performed to assess the effect of IBC on cell proliferation (Ki67), apoptosis (Cleaved-caspase 3) and tumor angiogenesis (CD31). Figure 2k ~ n showed the Ki-67 and CD31 expression were significantly decreased, while the expression level of Cleaved-caspase 3 were obviously increased as the IBC dose increased, indicating IBC could promote apoptosis and inhibit cell proliferation and tumor angiogenesis *in vivo*. Western blot analysis indicated the protein markers of apoptosis (AKT/p-AKT, Cleaved-caspase 3), inflammasome (ASC) and cell cycle (p21) were significantly changed after IBC treatment *in vivo*, suggesting the mechanism of IBC against GBM may be related to these processes and need to be further explored.

IBC is a novel potential regulatory of NLRP3

The mechanism of IBC inducing cell death of GBM cells was explored by network pharmacology. The 35 potential targets of IBC were screened out by GeneCards and SwissTargetPrediction databases, while 7223 targets of GBM were predicted by a comprehensive analysis of GeneCards and TCGA databases. The Venn diagram of these targets between IBC and GBM showed that 30 overlapping targets may be the potential treatment targets of IBC against GBM (Fig. 3a). The GO enrichment analysis found that these common targets enriched in 834 terms of biology process (BP), 32 terms of cellular component (CC) and 38 terms of molecular function (MF). The top 10 terms of BP, CC and MF were shown in Fig. 3b and Table S1. These common targets were related to response to metal ion (GO: 0010038), cellular response to metal ion (GO: 007124), peptidyl-serine phosphorylation (GO: 0018105), early endosome (GO: 0005769), membrane raft (GO:0098857), protein serine/threonine kinase activity (GO:0098857), phosphatase binding (GO:0019902) and protein serine/threonine/tyrosine kinase (GO:0004712). For KEGG analysis, Glioma, PI3K-Akt and MAPK signaling pathways were the main pathways for IBC treatment against GBM (Fig. 3c and Table S2). PPI analysis revealed that EGFR, AKT1, ESR1, MAPK1 and MAPK3 were the hub gene for IBC treatment (Fig. 3d ~ f). IBC-Targets-Pathways network were showed in Fig. 3g. Previous studies indicated that NLRP3 inducing inflammasome activation was the key driver of inflammatory cell death[23]. The 15 transcription factors (TF) targeting NLRP3 were predicted by NetworkAnalyst databases (Fig. 3h). By taking intersecting of TFs and hub genes of IBC against GBM, ESR1 were found

to be potential target of IBC regulating NLRP3 to mediate inflammatory cell death in GBM (Fig. 3i). The molecule docking of IBC with ESR1, AKT1 and MAPK1 were displayed in Fig. 3j ~ k. These results revealed IBC may target ESR1 (one of NLRP3 TFs), AKT1 and MAPK1 (NLRP3 upstream regulatory molecules) to stimulate proliferation-related pathways to inhibit GBM.

IBC reduced NLRP3 inflammasome-mediated pyroptosis and arrested the cell cycle at the G1 phase

NLRP3 inflammasome complex, consisting of the NLRP3, ASC adaptor and procaspase 1, triggering downstream inflammatory factor L-1β and IL-18 production and pyroptosis, plays a vital role of several neuroinflammatory diseases and cancer. The western blot results indicated that IBC downregulated NF-kB, NLRP3 inflammasome (NLRP3, ASC and pro-caspase 1), caspase 1, GSDMD, inflammatory factors (IL-18 and IL-1β) in U87MG and U251 cells in dose-dependent manner, suggesting IBC attenuated NLRP3 inflammasome-mediated inflammation response and pyroptosis in GBM (Fig. 4a ~ c). In addition, TNFα, a NF-kB-activated downstream cytokine that has been implicated in inflammation and glioma growth, were also reduced by IBC treatment. These results indicated that IBC may exhibit anti-inflammation and pyroptosis inhibition effects on GBM. To assess the potential effects of IBC on the cell cycle progression, U87MG cells with IBC treatment were conducted a flow cytometry-based cell cycle assay. As shown in Fig. 4d ~ e, IBC caused an increase in the G1 phase U87MG cells and a decrease in the S and G2 phase cells of U87MG cells, implying that IBC was able to arrest the cell cycle at the G1 phase in a dose-dependent manner. Moreover, with increasing IBC concentration in GBM cells, cell cycle regulator p53 and cyclin-dependent kinase inhibitor p21 protein levels were increased, while the levels of cyclin-dependent kinase 2 (CDK2) were decreased (Fig. 4f ~ h). These implied IBC caused pyroptosis inhibition and cell cycle arresting of GBM.

IBC induced mitochondria-dependent apoptosis in GBM cells

To validate the specific mechanisms of IBC against GBM, the ability of IBC to induce apoptosis was assessed by flow cytometry and fluorescence microscopy using Annexin V/Propidium Iodide (PI) staining (Fig. 5a ~ b). The proportion of early apoptotic cells (Annexin V^+/PI^- cells) significantly increased with increasing IBC concentration (Fig. 5a ~ c, e ~ g). The morphological changes with chromatin condensation and nuclear fragmentation in U87MG and U251 were also observed after IBC treatments for 48 h by Hoechst 33342 staining (Fig. 5d). Early apoptosis is usually accompanied by mitochondrial membrane potential changes[23]. Subsequently, JC-1 dye were used to measure mitochondrial membrane potential changes. As shown in Fig. 5h ~ i, U87MG and U251 treated with increasing IBC concentration exerted an increase in JC-1 monomers (green) and a decrease in JC-1 aggregates (red), as would be expected for early apoptosis. The mitochondrial membrane potential is regulated by the Bcl-2 family proteins, including pro-apoptotic Bax and anti-apoptotic Bcl-2 proteins. Then the effects of IBC on the levels of Bcl-2 family proteins were conducted by western blot analysis (Fig. 5j ~ l). The results showed IBC decreased significantly the expression of Bcl-2 in U87MG and U251, and increased Bax expression that was not statistically significant, while increasing the level of pro-apoptotic Cleaved-caspase 3, suggesting the mitochondria-dependent apoptosis occurred. Meanwhile, EGFR/PI3K/AKT

pathway is another well-known marker pathway regulating cell proliferation and usually sustaining activation in tumor cells. Figure 5j ~ l were also exerted IBC consistently reduced the levels of p-EGFR, PI3K, AKT, p-AKT, GSK-3β and p-GSK-3β in a dose-dependent manner. All these results indicated IBC induced mitochondria-dependent apoptosis in GBM cells.

The inhibitory effect of IBC on GBM was blocked by pan-caspase inhibitor Z-VAD-FMK

Cells can die through several distinct regulated cell death pathways, including apoptosis, pyroptosis, necrosis, ferroptosis, and so on. The connection between these cell death pathways were complicated. The caspase family members played a vital role of cross-talks between apoptosis and pyroptosis. Z-VAD-FMK was one of the pan-caspase inhibitors, which could reverse the apoptotic effect and inhibit pyroptosis [24]. In Fig. 6a ~ g, Z-VAD-FMK could prevent cell death triggered by IBC. In detail, the CCK-8 assay and cell morphology observation under the microscope showed Z-VAD-FMK could reverse the cytotoxic effects reverse and the morphological change induced by IBC in both U87MG and U251 cells (Fig. 6a ~ b). Similarly, Annexin V-PI double staining implied that Z-VAD-FMK blocked the apoptotic effects performed by IBC on both U87MG and U251 cells (Fig. 6d ~ g). These results further demonstrated that IBC could inhibit the growth of GBM cells by inducing apoptotic cell death.

Discussion

GBM is the primary brain tumor with the most aggressive malignancy, the worst clinical prognosis, and is easy to recurrence contributing to the high mortality. TMZ is the clinical first-line therapeutic drug approved for GBM treatment, However, secondly resistance to TMZ appears inevitable, and no effective treatment for TMZ-resistant recurrent GBM is available, ultimately leading to the failure of GBM treatment[8]. In this study, we have found, through both *in vitro* and *in vivo* assays, that IBC had potential anti-GBM activity. In particular, compared with the effectiveness of TMZ, IBC had higher treatment efficacy and lower required drug doses in vitro. These results provided a reliable basis for the feasibility of IBC treatment for GBM.

IBC, a naturally occurring chalcone, is one of the main active compounds of *Psoralea corylifolia Linn* which is a widely used traditional Chinese medicine and Ayurvedic herbal medicine in India[9]. Accumulative studies have confirmed the inhibitory effects of IBC on several cancers both in vitro and in vivo models [9]. Consistent with the previous findings, our study showed a significant decrease in cell proliferation in vitro and in vivo GBM models treated with IBC, suggesting anti-GBM activities of IBC. Moreover, our study also proved that IBC exerted an inhibitory effect on the migration and invasion of GBM cells in vitro. This is consistent with the findings in tongue squamous cell carcinoma cells [25]. It had been proved that IBC could reduce matrix metalloproteinase-2 (MMP-2) and MMP-9 protein levels, resulting in inhibition of the migration and invasion of tongue squamous cell carcinoma in vitro[25]. However, the precise mechanism of IBC inhibition on migration and invasion in GBM awaits further clarification. In vivo, IBC also displayed a significant tumor inhibitory effects in GBM xenograft mice without obvious toxicity. A similar phenomenon was also observed in acute myeloid leukemia (AML)

xenograft mice treated with IBC[26]. In AML, IBC oral administration suppressed tumor growth in HL60 xenograft mice with little toxicity[27, 26]. These results implicated IBC exhibited a relative low-systemic toxicity in vivo. The low cytotoxicity of IBC to normal cells, such as hepatocytes, normal liver cells, umbilical vein endothelial cells, and cerebellar granule cells, were also observed in a previous research[28, 9, 29]. These studies were in agreement with the effects of IBC in retarding the growth of a wide range of cancer cells and tumors while protecting normal cells and tissues in vitro and in vivo.

The anti-cancer effect of IBC is mainly mediated by cell death induction, including apoptosis, methuosis-like cell death or autophagy-related cell death[9]. In our study, IBC were predicted to interact with ESR1 (estrogen receptor 1) which was the transcription factors of NLRP3 by network pharmacology and molecule docking analysis. NLRP3 plays a vital role in pyroptosis which is a programmed cell death (PCD) characterized by the activation of inflammatory caspases, including caspase 1 and caspase 4/5 (caspase 11 in mice), and release of pro-inflammatory cytokines, including mature IL-1β and IL-18[30, 31]. Classical pyroptosis pathway is generally shown as an inflammasome complex containing caspase 1 precursors was firstly formed by inflammasome sensors NLRP3, AIM2 or Pyrin combining with inflammasome adaptor protein ASC, and that precursor of caspase 1 is then sheared to produce active caspase 1, leading to cleavage of the substrate Gasdermin D and production of N-terminal fragment of Gasdermin D and pyroptosis finally[30]. Surprisingly, our further experiments found IBC inhibited rather than promoted pyroptosis by downregulating classical NLRP3 inflammasome dependent pyroptosis pathway (NLRP3/ASC/Caspase 1/Gasdermin D) and causing reduced releases of IL-1β and IL-18. Considering that pyroptosis is an inflammatory cell death and plays a vital role in the pathophysiology of several inflammatory disorders, including neurological and metabolic disorders, chronic inflammatory diseases, and cancer, we proposed anti-GBM effects of IBC may be mediated by reducing inflammatory factors to decrease inflammation or by another PCD. Our further study revealed that another remarkable inflammatory factors TNFα were also downregulated by IBC treatment in GBM cells, which provided further, albeit indirect, evidence of above speculation.

Several proteins may be the potential targets for the anti-cancer effect of IBC[9]. Beside ESR1 molecule, EGFR, AKT1 and MAPK1 were the hub genes for IBC treatment against GBM by network pharmacology and molecule docking analysis. In IBC-treated GBM cells, the levels of p-EGFR, PI3K, AKT, p-AKT, GSK-3β and p-GSK-3β were also decreased. In previous researches, IBC had been identified to be a potent inhibitor of protein kinase B (PKB/AKT). It could bind with the ATP site of AKT and inhibit the AKT kinase activity via abating AKT phosphorylation at Ser-473. It also blocked AKT translocation from the cytoplasm to the nucleus. This led to mitochondria-mediated apoptosis of several lines of cancer cells[32]. Inhibition of AKT by IBC causes suppression of the glycogen synthase kinase 3β (GSK-3β)/β-catenin signaling pathway, which results in apoptosis in colorectal cancer cells[29]. Furthermore, IBC also showed inhibitory effects on estrogen receptor (ER) in ER^+ breast cancer and prostate cancer cells [33]. It had been proved that activation of PI3K leads to activation of AKT, which can directly activate ESR to promote transcription of target genes in ligand-independent manner and endocrine therapy resistance[34, 35]. On the contrary, inhibition of AKT by IBC could also inactivate ESR to downregulate NLRP3 mRNA

transcription. In addition, we also found that IBC could also regulatep53, p21 and CDK2 protein expressions to arrest the cell cycle at G1 phase of GBM cells.

Our results found that IBC induced mitochondria-mediated apoptosis in GBM cells via Bcl-2/Caspase 3 pathway, which is consistent with previous studies. Additionally, apoptotic executioner caspases, caspase 3 and caspase 7, are reported to inactivate pyroptotic GSDMD through N-terminal cleavage[36]. However, these caspases are also reported shift the morphology of cell death from apoptotic to pyroptotic through cleavage of another member of the gasdermin family, gasdermin E (GSDME), also known as DFNA5[37]. It is also clear that other pyroptotic molecules, such as caspase 1, can regulate apoptosis and the cleavage of apoptotic substrates, while apoptotic molecules caspase 8 and FADD can regulate pyroptosis activation. These and other observations make it clear that there are numerous molecular connections between the cell death pathways that may complicate the development of therapeutics. However, these molecular connections could certainly be related with the proteins of Caspase family members. In our study, pan-caspase inhibitor (Z-VAD-FMK) could prevent cell death triggered by IBC, suggesting the mechanism of IBC against GBM may also be more complex than those we observed. The precise anti-cancer mechanism of IBC still require further investigation.

Conclusions

In summary, our results demonstrated that IBC inhibit GBM cell proliferation, migration and invasion *in vitro* in a dose-dependent manner and prevent tumor growth without any significant drug toxicity *in vivo*. Mechanistic studies further suggested that IBC could reduce NLRP3 inflammasome-related pyroptosis and inflammation by targeted ESR1, arrest cell cycle at G1 phase, and induce mitochondria-dependent apoptosis in GBM cells (Fig. 6h). Therefore, IBC may be a particularly effective strategy for GBM therapy.

Declarations

Acknowledgements

Not applicable

Author Contributions

Yueshan Wu, Ni Zhu and Meichun Hu conceived the study. Yueshan Wu, Jing Chang, Juanjuan Ge, Kangyan Xu, Quan Zhou and Meichun Hu designed, performed, and analyzed experiments. Kangyan Xu performed all animal model assays for the study. Quan Zhou and Xiaowen Zhang provided bioinformatics analysis and reagent preparations. Ni Zhu and Meichun Hu provided critical feedback, contributed to manuscript preparation, and oversaw the research program. All authors listed reviewed the manuscript and provided feedback with writing and revisions.

Funding

This work was supported by grants from the National Natural Science Foundation of China (no.81602649), the Natural Science Foundation of Hubei Province (2018CFB173), the Scientific projects of health commission of Hubei Province (WJ2019Q022/WJ2021M089), The Foundation of the Hubei University of Science and Technology (2020TD04/2021-23GP04/2021WG02), National Training Program of Innovation and Entrepreneurship for Undergraduates (S201910927040/202110927002).

Data Availability

All data generated or analyzed during this study are included in this published article. Requests for material should be made to the corresponding authors.

Human and Animal Rights and Informed Consent

All procedures performed in studies involving animals were in accordance with the ethical standards of the institution or practice at which the studies were conducted.

Consent to Participate

Not applicable.

Consent for Publication

Not applicable.

Competing Interests

The authors declare no competing interests.

References

1. Puchalski R, Shah N, Miller J, Dalley R, Nomura S, Yoon J, Smith K, Lankerovich M, Bertagnolli D, Bickley K, Boe A, Brouner K, Butler S, Caldejon S, Chapin M, Datta S, Dee N, Desta T, Dolbeare T, Dotson N, Ebbert A, Feng D, Feng X, Fisher M, Gee G, Goldy J, Gourley L, Gregor B, Gu G, Hejazinia N, Hohmann J, Hothi P, Howard R, Joines K, Kriedberg A, Kuan L, Lau C, Lee F, Lee H, Lemon T, Long F, Mastan N, Mott E, Murthy C, Ngo K, Olson E, Reding M, Riley Z, Rosen D, Sandman D, Shapovalova N, Slaughterbeck C, Sodt A, Stockdale G, Szafer A, Wakeman W, Wohnoutka P, White S, Marsh D, Rostomily R, Ng L, Dang C, Jones A, Keogh B, Gittleman H, Barnholtz-Sloan J, Cimino P, Uppin M, Keene C, Farrokhi F, Lathia J, Berens M, Iavarone A, Bernard A, Lein E, Phillips J, Rostad S, Cobbs C, Hawrylycz M, Foltz G (2018) An anatomic transcriptional atlas of human glioblastoma. Science (New York, NY) 360 (6389):660-663. doi:10.1126/science.aaf2666
2. Siegel R, Miller K, Fuchs H, Jemal A (2022) Cancer statistics, 2022. CA: a cancer journal for clinicians 72 (1):7-33. doi:10.3322/caac.21708

3. Bausart M, Préat V, Malfanti A (2022) Immunotherapy for glioblastoma: the promise of combination strategies. Journal of experimental & clinical cancer research : CR 41 (1):35. doi:10.1186/s13046-022-02251-2
4. Davis B, Shen Y, Poon C, Luchman H, Stechishin O, Pontifex C, Wu W, Kelly J, Blough M (2016) Comparative genomic and genetic analysis of glioblastoma-derived brain tumor-initiating cells and their parent tumors. Neuro-oncology 18 (3):350-360. doi:10.1093/neuonc/nov143
5. Gregory J, Kadiyala P, Doherty R, Cadena M, Habeel S, Ruoslahti E, Lowenstein P, Castro M, Lahann J (2020) Systemic brain tumor delivery of synthetic protein nanoparticles for glioblastoma therapy. Nature communications 11 (1):5687. doi:10.1038/s41467-020-19225-7
6. Tan A, Ashley D, López G, Malinzak M, Friedman H, Khasraw M (2020) Management of glioblastoma: State of the art and future directions. CA: a cancer journal for clinicians 70 (4):299-312. doi:10.3322/caac.21613
7. Sang Y, Hou Y, Cheng R, Zheng L, Alvarez A, Hu B, Cheng S, Zhang W, Li Y, Feng H (2019) Targeting PDGFRα-activated glioblastoma through specific inhibition of SHP-2-mediated signaling. Neuro-oncology 21 (11):1423-1435. doi:10.1093/neuonc/noz107
8. Chen X, Zhang M, Gan H, Wang H, Lee J, Fang D, Kitange G, He L, Hu Z, Parney I, Meyer F, Giannini C, Sarkaria J, Zhang Z (2018) A novel enhancer regulates MGMT expression and promotes temozolomide resistance in glioblastoma. Nature communications 9 (1):2949. doi:10.1038/s41467-018-05373-4
9. Wang M, Lin L, Lu J, Chen X (2021) Pharmacological review of isobavachalcone, a naturally occurring chalcone. Pharmacological research 165:105483. doi:10.1016/j.phrs.2021.105483
10. Yang Y, Zhang Y, Chen Z, Zhang Y, Yang X (2018) Plasma pharmacokinetics and cerebral nuclei distribution of major constituents of Psoraleae fructus in rats after oral administration. Phytomedicine : international journal of phytotherapy and phytopharmacology 38:166-174. doi:10.1016/j.phymed.2017.12.002
11. Jing H, Wang S, Wang M, Fu W, Zhang C, Xu D (2017) Isobavachalcone Attenuates MPTP-Induced Parkinson's Disease in Mice by Inhibition of Microglial Activation through NF-κB Pathway. PloS one 12 (1):e0169560. doi:10.1371/journal.pone.0169560
12. Zhang M, Wu Q, Zhao R, Yao X, Du X, Liu Q, Lv G, Xiao S (2021) Isobavachalcone ameliorates cognitive deficits, and Aβ and tau pathologies in triple-transgenic mice with Alzheimer's disease. Food & function 12 (17):7749-7761. doi:10.1039/d1fo01306h
13. Wu R, Young I, Chen Y, Chuang S, Toubaji A, Wu M (2019) Identification of the PTEN-ARID4B-PI3K pathway reveals the dependency on ARID4B by PTEN-deficient prostate cancer. Nature communications 10 (1):4332. doi:10.1038/s41467-019-12184-8
14. Ku A, Hu H, Zhao X, Shah K, Kongara S, Wu D, McCormick F, Balmain A, Bandyopadhyay S (2020) Integration of multiple biological contexts reveals principles of synthetic lethality that affect reproducibility. Nature communications 11 (1):2375. doi:10.1038/s41467-020-16078-y

15. Shin S, Kim K, Kim H, Ylaya K, Do S, Hewitt S, Park H, Roe J, Chung J, Song J (2020) Deubiquitylation and stabilization of Notch1 intracellular domain by ubiquitin-specific protease 8 enhance tumorigenesis in breast cancer. Cell death and differentiation 27 (4):1341-1354. doi:10.1038/s41418-019-0419-1
16. Fekry B, Ribas-Latre A, Baumgartner C, Deans J, Kwok C, Patel P, Fu L, Berdeaux R, Sun K, Kolonin M, Wang S, Yoo S, Sladek F, Eckel-Mahan K (2018) Incompatibility of the circadian protein BMAL1 and HNF4α in hepatocellular carcinoma. Nature communications 9 (1):4349. doi:10.1038/s41467-018-06648-6
17. Nayak D, Kumar A, Chakraborty S, Rasool R, Amin H, Katoch A, Gopinath V, Mahajan V, Zilla M, Rah B, Gandhi S, Ali A, Kumar L, Goswami A (2017) Inhibition of Twist1-mediated invasion by Chk2 promotes premature senescence in p53-defective cancer cells. Cell death and differentiation 24 (7):1275-1287. doi:10.1038/cdd.2017.70
18. Park S, Kim J, Kang S, Cha H, Shin H, Park J, Jang Y, Woo J, Won C, Min D (2020) Discovery of direct-acting antiviral agents with a graphene-based fluorescent nanosensor. Science advances 6 (22):eaaz8201. doi:10.1126/sciadv.aaz8201
19. Arif T, Krelin Y, Nakdimon I, Benharroch D, Paul A, Dadon-Klein D, Shoshan-Barmatz V (2017) VDAC1 is a molecular target in glioblastoma, with its depletion leading to reprogrammed metabolism and reversed oncogenic properties. Neuro-oncology 19 (7):951-964. doi:10.1093/neuonc/now297
20. Shannon P, Markiel A, Ozier O, Baliga N, Wang J, Ramage D, Amin N, Schwikowski B, Ideker T (2003) Cytoscape: a software environment for integrated models of biomolecular interaction networks. Genome research 13 (11):2498-2504. doi:10.1101/gr.1239303
21. Chin C, Chen S, Wu H, Ho C, Ko M, Lin C (2014) cytoHubba: identifying hub objects and sub-networks from complex interactome. BMC systems biology:S11. doi:10.1186/1752-0509-8-s4-s11
22. Trott O, Olson A (2010) AutoDock Vina: improving the speed and accuracy of docking with a new scoring function, efficient optimization, and multithreading. Journal of computational chemistry 31 (2):455-461. doi:10.1002/jcc.21334
23. Christgen S, Place D, Kanneganti T (2020) Toward targeting inflammasomes: insights into their regulation and activation. Cell research 30 (4):315-327. doi:10.1038/s41422-020-0295-8
24. Kapoor S, Natarajan K, Baldwin P, Doshi K, Lapidus R, Mathias T, Scarpa M, Trotta R, Davila E, Kraus M, Huszar D, Tron A, Perrotti D, Baer M (2018) Concurrent Inhibition of Pim and FLT3 Kinases Enhances Apoptosis of FLT3-ITD Acute Myeloid Leukemia Cells through Increased Mcl-1 Proteasomal Degradation. Clinical cancer research : an official journal of the American Association for Cancer Research 24 (1):234-247. doi:10.1158/1078-0432.Ccr-17-1629
25. Shi Y, Wu W, Huo A, Zhou W, Jin X (2017) Isobavachalcone inhibits the proliferation and invasion of tongue squamous cell carcinoma cells. Oncology letters 14 (3):2852-2858. doi:10.3892/ol.2017.6517
26. Wu D, Wang W, Chen W, Lian F, Lang L, Huang Y, Xu Y, Zhang N, Chen Y, Liu M, Nussinov R, Cheng F, Lu W, Huang J (2018) Pharmacological inhibition of dihydroorotate dehydrogenase induces

apoptosis and differentiation in acute myeloid leukemia cells. Haematologica 103 (9):1472-1483. doi:10.3324/haematol.2018.188185

27. He H, Wang C, Liu G, Ma H, Jiang M, Li P, Lu Q, Li L, Qi H (2021) Isobavachalcone inhibits acute myeloid leukemia: Potential role for ROS-dependent mitochondrial apoptosis and differentiation. Phytotherapy research : PTR 35 (6):3337-3350. doi:10.1002/ptr.7054
28. Li B, Xu N, Wan Z, Ma L, Li H, Cai W, Chen X, Huang Z, He Z (2019) Isobavachalcone exerts anti-proliferative and pro-apoptotic effects on human liver cancer cells by targeting the ERKs/RSK2 signaling pathway. Oncology reports 41 (6):3355-3366. doi:10.3892/or.2019.7090
29. Li Y, Qin X, Li P, Zhang H, Lin T, Miao Z, Ma S (2019) Psoralea corylifoliaIsobavachalcone isolated from inhibits cell proliferation and induces apoptosis via inhibiting the AKT/GSK-3β/β-catenin pathway in colorectal cancer cells. Drug design, development and therapy 13:1449-1460. doi:10.2147/dddt.S192681
30. Christgen S, Tweedell R, Kanneganti T (2021) Programming inflammatory cell death for therapy. Pharmacology & therapeutics:108010. doi:10.1016/j.pharmthera.2021.108010
31. Morris G, Walker A, Berk M, Maes M, Puri B (2018) Cell Death Pathways: a Novel Therapeutic Approach for Neuroscientists. Molecular neurobiology 55 (7):5767-5786. doi:10.1007/s12035-017-0793-y
32. Jing H, Zhou X, Dong X, Cao J, Zhu H, Lou J, Hu Y, He Q, Yang B (2010) Abrogation of Akt signaling by Isobavachalcone contributes to its anti-proliferative effects towards human cancer cells. Cancer letters 294 (2):167-177. doi:10.1016/j.canlet.2010.01.035
33. Shi J, Chen Y, Chen W, Tang C, Zhang H, Chen Y, Yang X, Xu Z, Wei J, Chen J (2018) Isobavachalcone sensitizes cells to E2-induced paclitaxel resistance by down-regulating CD44 expression in ER+ breast cancer cells. Journal of cellular and molecular medicine 22 (11):5220-5230. doi:10.1111/jcmm.13719
34. Khatpe A, Adebayo A, Herodotou C, Kumar B, Nakshatri H (2021) Nexus between PI3K/AKT and Estrogen Receptor Signaling in Breast Cancer. Cancers 13 (3). doi:10.3390/cancers13030369
35. Niedzielska E, Smaga I, Gawlik M, Moniczewski A, Stankowicz P, Pera J, Filip M (2016) Oxidative Stress in Neurodegenerative Diseases. Molecular neurobiology 53 (6):4094-4125. doi:10.1007/s12035-015-9337-5
36. de Vasconcelos N, Van Opdenbosch N, Van Gorp H, Martín-Pérez R, Zecchin A, Vandenabeele P, Lamkanfi M (2020) An Apoptotic Caspase Network Safeguards Cell Death Induction in Pyroptotic Macrophages. Cell reports 32 (4):107959. doi:10.1016/j.celrep.2020.107959
37. Rogers C, Fernandes-Alnemri T, Mayes L, Alnemri D, Cingolani G, Alnemri E (2017) Cleavage of DFNA5 by caspase-3 during apoptosis mediates progression to secondary necrotic/pyroptotic cell death. Nature communications 8:14128. doi:10.1038/ncomms14128

Figures

Figure 1

IBC inhibited proliferation, migration and invasion of GBM cells in dose-dependent manner. (a) The structure of IBC. (b) U87MG and U251 cells were treated with the increasing doses of IBC for 48 h. Cell viability were assessed by MTT assay. (c) The morphology of U87MG and U251 cells after IBC treatment for 48 h. (d) The structure of TMZ. (e) U87MG and U251 cells were treated with the increasing doses of TMZ for 48 h. Cell viability were measured by MTT assay. (f) The morphology of U87MG and U251 cells after TMZ treatment for 48 h. (g~h) U87MG and U251 cells were treated with the indicated concentrations of IBC for 7 days. Colony formation was determined by crystal violet staining. The statistical results of colony numbers were presented in (I) and (J). (k~l) Wound healing assays of U87MG and U251 cells after IBC treatment. U87MG and U251 cells were cultured until confluence, and a scratch was made in the cell layer. After IBC treatment for 48 h, the images of U87MG and U251 cells were taken by light microscope. Cell migration rates were statistically analyzed. (m~n) U87MG and U251 cells images after Wound healing assays. (o~t) Transwell invasion and migration assay of U87MG and U251 cells after IBC treatment. U87MG cells or U251 cells were seeded on the upper chamber of Transwell. After 48 h incubation with IBC (0.5, 1 and 2 μM in U87MG or 0.25, 0.5 and 1 μM in U251), migratory and invasive cells were stained and counted (o, r). (p~q, s~t) Quantification of U87MG cells migration and invasion rates through the membrane per field in (o, r). Data were presented as mean ± SD or as a representative images of triplicate experiments, *P<0.05, **P<0.01 by one-way ANOVA with Tukey's post-hoc test. Scale bars, 100 μm.

Figure 2

IBC suppressed the tumor growth of GBM xenograft mice. (a) Scheme of the experimental workflow. Firstly, GBM Xenograft tumor model were established by subcutaneous injection with 5×10^6 U87MG cells. 14 days later, xenograft mice delivered daily with DMSO, 20 mg/kg or 40 mg/kg IBC by intragastric administration (n=10 per group), respectively. After 14 days administration, mice were sacrificed, and the samples were prepared for following tests. (b) Images of GBM xenograft mice. (c) Images of xenograft tumor. (d) Tumor volumes curve during IBC administration period. (e) Tumor weights at experimental endpoint. (f) Body weights curve during IBC administration period. (g) Vascular area changes of the IBC-treated xenograft mice. (h) Livers images of the IBC-treated xenograft mice. (I) Liver/body ratios of the xenograft mice with IBC treatment. (j) HE staining of heart, liver, spleen, lung and kidney of the xenograft mice with IBC treatment. (k) HE staining and IHC with antibody against Ki-67, Cleaved-caspase 3 and CD31 of tumor tissues. (l~n) Quantification of HE and IHC in (k). (o) Western blot analysis of the indicated proteins expression levels in xenograft tumor tissues. (p) Quantification of western blot in (o). Data were presented as mean ± SD or as a representative images, *P<0.05, **P<0.01 vs. the control group

by one-way ANOVA with Tukey's post-hoc test or two-way RM ANOVA with Sidak’s multiple comparisions test. Scale bars, 100 μm.

Figure 3

The effective targets of IBC against GBM predicted by network pharmacology analysis. The IBC molecular structure was obtained from Pubchem database, then the structure were imput into SwissTargetPrediction database to predict relevant targets of IBC for Homo sapiens based on its chemical structure. The GBM disease-related targets were retrieved from the GeneCards database by using the keywords “glioma”. (a) The overlapped IBC-GBM targets were screened out by Venny 2.1.0. (b) The GO functional enrichments of overlapped IBC-GBM targets were analyzed by R (v.3.6.3) software. (c) The KEGG pathway enrichments of overlapped IBC-GBM targets were also performed by R (v.3.6.3) software. (d) The PPI network of the IBC-GBM targets were conducted by STRING database. (e~g) The PPI network (e), the Top 10 hub gene (f), IBC-Targets-Pathway (g) were calculated and displayed by Cytoscape (3.8.0) software. (h) The interaction network of NLRP3 transcription factors (TFs) was obtained in Gene Regulatory Networks. (i) Venn diagram of IBC-related targets, GBM-related targets and predictive NLRP3 TFs were taken by Venny 2.1.0. (j~l) the molecular docking of IBC with ESR1 (j), Akt1(k) and EGFR (l) were obtained by Autodock-VINA and Pymol softwares.

Figure 4

IBC reduced pyroptosis in GBM cells and arrested the cell cycle at the G1 phase. (a) U87MG and U251 cells were treated with the increasing doses of IBC for 48 h, the indicated proteins were analyzed by western blot. The statistical results of western blot in U87MG and U251 were shown in (b) and (c). (d) U87MG and U251 cells cycles were measured by flow cytometry after IBC treatment for 48 h. the results of flow cytometry was presented in (e). (f~g) The cell cycle-related proteins were analyzed by western blot after IBC treatment in U87MG and U251 cells for 48 h. The statistical results of western blot in U87MG and U251 were shown in (f) and (h), respectively. Data were presented as mean ± SD or as a representative images, *P<0.05, **P<0.01 vs. the control group by one-way ANOVA with Tukey's post-hoc test.

Figure 5

IBC triggered mitochondria-dependent apoptosis in GBM cells. (a~c) U87MG and U251 cells were treated with IBC at indicated doses for 48 h, then the apoptosis cells were stained by Annexin V/Propidium Iodide (PI) and detected by flow cytometry in U87MG (a) and fluorescence microscopy in U87MG (b) and U251

cells (c). (d) Hoechst 33342 staining of U87MG and U25 cells with IBC treatments for 48 h. The statistics of (a~c) were shown in (e~g). (h~i) The mitochondrial membrane potential changes in U87MG (h) and U251 (i) cells after IBC treatments for 48 h. (j) U87MG and U251 cells were treated with the increasing doses of IBC for 48 h, the indicated proteins were analyzed by western blot. The statistical results of western blot in U87MG and U251 were shown in (k) and (l), respectively. Data were presented as mean ± SD or as a representative images, *P<0.05, **P<0.01 vs. the control group by one-way ANOVA with Tukey's post-hoc test.

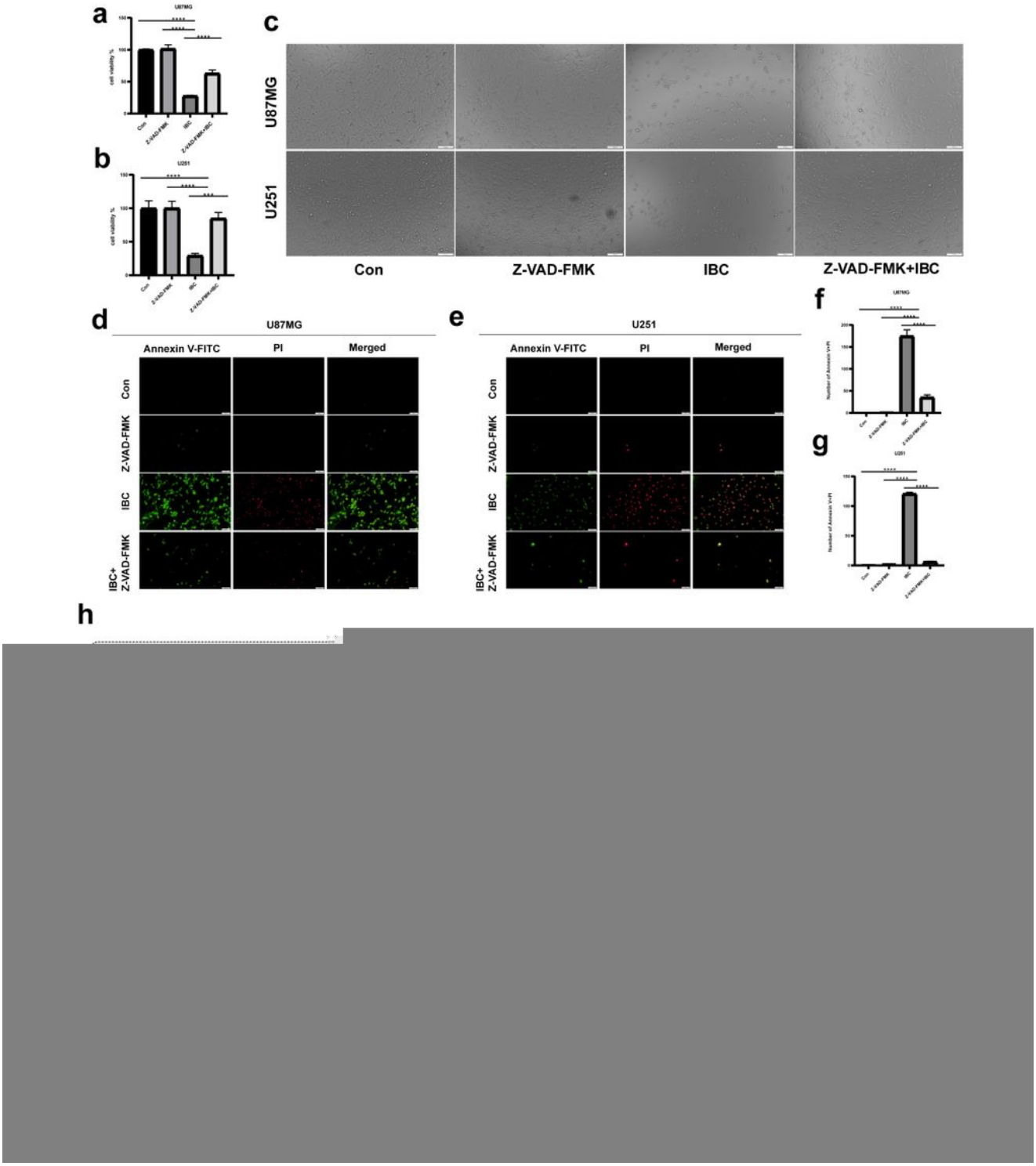

Figure 6

The anti-GBM activity of IBC was blocked by Z-VAD-FMK. U87MG and U251 cells were treated with IBC (μM), Z-VAD-FMK (μM) and IBC (μM) + Z-VAD-FMK (μM) for 48 h, respectively. (a~b) The CCK-8 assay were used to analyze the cell viability of U87MG (a) and U251 cells (b). (c) The morphological change in U87MG and U251 cells after IBC and Z-VAD-FMK treatment for 48 h. (d~e) The cell apoptosis changes in U87MG (d) and U251 (e) cells after IBC and Z-VAD-FMK treatment for 48 h were performed by Annexin V-FITC/PI double staining assay. (h) Schematic model for the mechanism of anti-GBM activity of IBC. IBC reduced NLRP3 inflammasome-related pyroptosis and inflammation via NLRP3/ASC/Caspase 1/Gasdermin D pathway, arrest cell cycle at G1 phase via p53/p21/CDK2 pathway, and induce mitochondria-dependent apoptosis in GBM cells. *P<0.05, **P<0.01 vs. the control group by one-way ANOVA with Tukey's post-hoc test.

Supplementary Files

This is a list of supplementary files associated with this preprint. Click to download.

- Supplementarytables.xlsx